JACS
JOURNAL OF THE AMERICAN CHEMICAL SOCIETY
pubs.acs.org/JACS
Article

Ordered Van der Waals Hetero-nanoribbon from Pressure-Induced Topochemical Polymerization of Azobenzene

Peijie Zhang,○ Dexiang Gao,○ Xingyu Tang, Xin Yang, Haiyan Zheng, Yida Wang, Xuan Wang, Jingqin Xu, Zijia Wang, Jie Liu, Xiaoge Wang, Jing Ju, Mingxue Tang, Xiao Dong, Kuo Li,* and Ho-kwang Mao

Cite This: J. Am. Chem. Soc. 2023, 145, 6845−6852
Read Online
ACCESS | Metrics & More | Article Recommendations | Supporting Information

ABSTRACT: Pressure-induced topochemical polymerization of molecular crystals with various stackings is a promising way to synthesize materials with different co-existing sub-structures. Here, by compressing the azobenzene crystal containing two kinds of intermolecular stacking, we synthesized an ordered van der Waals carbon nanoribbon (CNR) heterostructure in one step. Azobenzene polymerizes via a [4 + 2] hetero-Diels−Alder (HDA) reaction of phenylazo-phenyl in layer A and a *para*-polymerization reaction of phenyl in layer B at 18 GPa, as evidenced by in situ Raman and IR spectroscopies, X-ray diffraction, as well as gas chromatography−mass spectrometry and the solid-state nuclear magnetic resonance of the recovered products. The theoretical calculation shows that the obtained CNR heterostructure has a type II (staggered) band gap alignment. Our work highlights a high-pressure strategy to synthesize bulk CNR heterostructures.

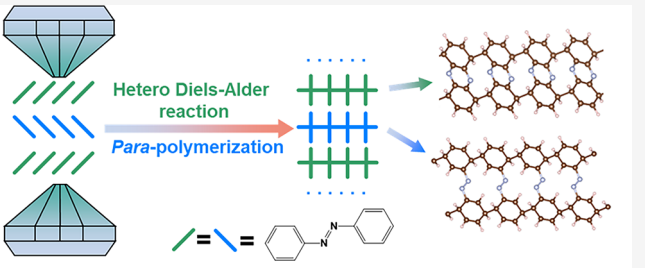

From Azobenzene to Ordered van der Waals Hetero-Nanoribbons

INTRODUCTION

A van der Waals (vdW) heterostructure is constructed by two or more materials with distinct chemical compositions, structures, or properties, which has gained wide attention from fundamental physics and chemistry to the materials science like optoelectronics, electrocatalysis, and energy storage.[1,2] Its exceptional properties are highly related to the structure of individual components and their stackings.[3−6] For example, the placement of graphene on top of BN improved the charge carrier mobility of devices,[7] and the carbon nanotube/graphene vdW heterostructure phototransistor exhibits high photoresponsivity and fast operating speeds.[8] Until now, various synthetic strategies like sequent growth, self-assembly, and physical transfer have been explored to construct the heterostructures,[6,9,10] but bulk synthesis of the atomic-scale-ordered heterostructure materials is still a great challenge.

Pressure-induced polymerization (PIP) is a successful method for preparing carbon-based materials with extended structures[11−13] and has demonstrated its adaptability in the preparation of graphane,[14,15] ultra-thin diamond nanothreads,[16−21] nanoribbons,[22] as well as graphite−diamond composites.[23−26] Most PIP reactions proceed via a topochemical route, and the structure of the final product was highly related to the intermolecular conformation of its precursors.[27] That means, the molecular stacking is the key to determine the structure of the synthesized materials. For example, 1,4-diphenyl-1,3-butadiyne (DPB) polymerizes via a dehydro-Diels−Alder route at the closest intermolecular distance $d_{C\cdots C}$ = 3.2 Å, instead of the common 1,4-addition reaction of diacetylenes due to the long alkyne···alkyne distance.[22] Therefore, if a single-component crystal contains various molecular stackings, a novel carbon material with different extend sub-structures (vdW heterostructure) would be realized, like hetero-nanoribbons and hetero-nanothreads, which would provide adjustable and intriguing properties compared to the traditional heterostructures. Azobenzene, a well-known molecule, has exactly such a crystal structure.[28] As shown in Figure 1, in layer A, the molecules have a slipped stacking with the phenyl ring against the space between the azo and phenyl groups of the adjacent molecule, while in layer B, the molecules are stacked right against each other. Recently, azobenzene was reported to undergo an irreversible chemical process above 18 GPa, in which the whole molecule, rather than the individual N═N or C═C bond, undergoes an addition reaction.[29] In contrast, assuming the polymerization of the phenyl group, a double-core nanothread model was also proposed, with the azo group unreacted during the PIP and present in the recovered materials.[30,31] This discrepancy is

Received: December 25, 2022
Published: March 16, 2023

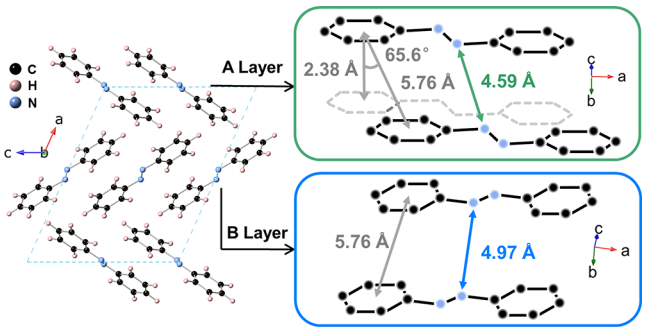

Figure 1. Crystal structure of azobenzene at ambient pressure and room temperature. The dashed line represents the projection of molecules in the above layer.

likely due to the complex crystal structure and makes the PIP of azobenzene an interesting topic. In this work, we found that the PIP of azobenzene proceeded via different reactions in its A and B layers, respectively, with a [4 + 2] hetero-Diels–Alder (HDA) reaction of phenylazo-phenyl in layer A and a *para*-polymerization reaction of phenyl in layer B. An orderly stacked vdW heterostructure with two kinds of carbon–nitrogen nanoribbons is the final product. Such a PIP of the crystal with different packings provides a straightforward route to construct bulk heterostructure materials.

RESULTS AND DISCUSSION

First, we investigated the onset of the PIP of azobenzene [purity confirmed by X-ray diffraction (XRD) as shown in Figure S1] by in situ Raman spectra. To avoid possible photoreactions or photoisomerization transitions, the laser with a wavelength of 785 nm was used for in situ measurement (Figure S2 using 532 nm for comparison). Upon compression, all the Raman peaks blue-shifted gradually and broadened above 10 GPa (Figures 2a and S3). A possible phase transition of azobenzene occurs around 10 GPa as indicated by frequency discontinuity with pressure (Figure S4).[29−31] The N═N stretching peak ($\nu_{N=N}$, at about 1460 cm^{-1}) splits into two peaks at about 1450 and 1467 cm^{-1}, respectively, above 19 GPa (Figure 2b). The first one at ∼1450 cm^{-1} then weakened together with the ν_{C-C} in phenyl (∼1600 cm^{-1}), indicating a chemical transformation involving azo and phenyl groups, which defines the onset of the reaction. On the other hand, the second $\nu_{N=N}$ peak located at ∼1467 cm^{-1} maintained until 31.8 GPa. This indicates that part of azo groups was involved in the reaction when compressed to 31 GPa. The recovered

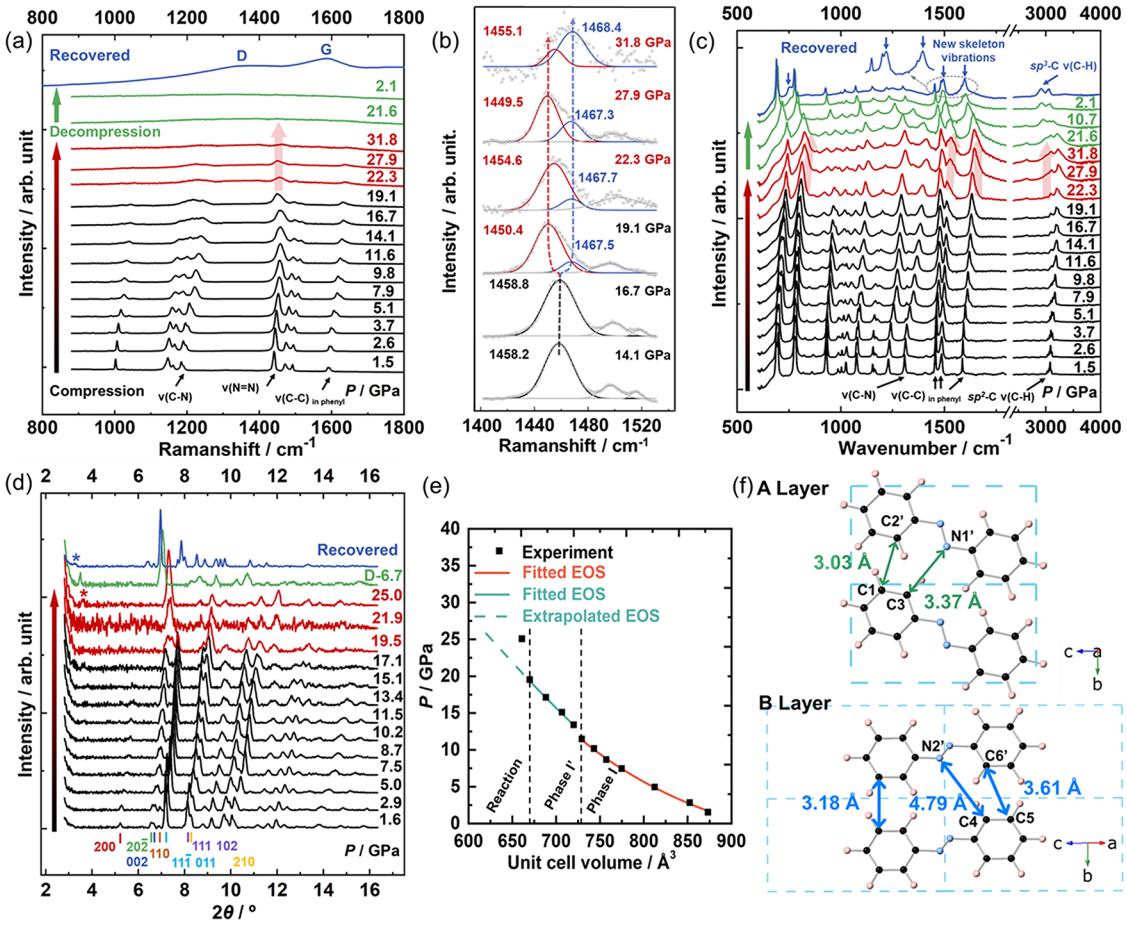

Figure 2. (a) In situ high-pressure Raman spectra of azobenzene. (b) Raman peak of $\nu_{N=N}$ under high pressure. The solid black, red, and blue lines stand for the fitting results of the $\nu_{N=N}$ peak, and the solid gray line stands for the fitting results of the ρ_{C-H} peak. The gray circles represent the experimental data. In situ high-pressure (c) IR spectra and (d) XRD of azobenzene (Raman and IR peak assignments in Table S1). ν and ρ represent the stretching and rocking vibration, respectively. The blue arrows in (c) and asterisks in (d) mark the new peaks during compression of azobenzene. D represents the decompression process. The XRD patterns up to 21.9 GPa were collected with an exposure time of 300 s, with 600 s for others. (e) Fitting of the EOS of azobenzene. (f) Intermolecular distances of azobenzene in A and B layers at 17.1 GPa.

https://doi.org/10.1021/jacs.2c13753
J. Am. Chem. Soc. 2023, 145, 6845−6852

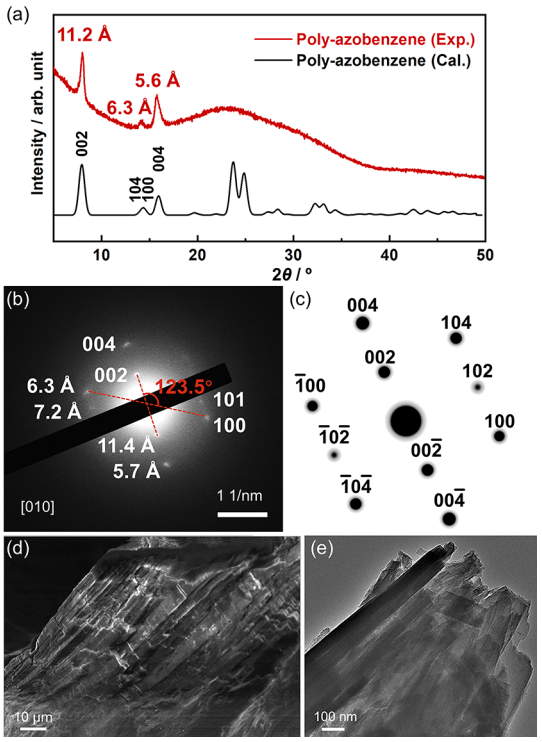

Figure 3. Crystallographic investigation on the poly-azobenzene. (a) XRD patterns of poly-azobenzene from the experiment and calculation. (b) SAED pattern of poly-azobenzene. (c) Simulated SAED pattern of poly-azobenzene along [010]. (d) SEM and (e) TEM image of poly-azobenzene.

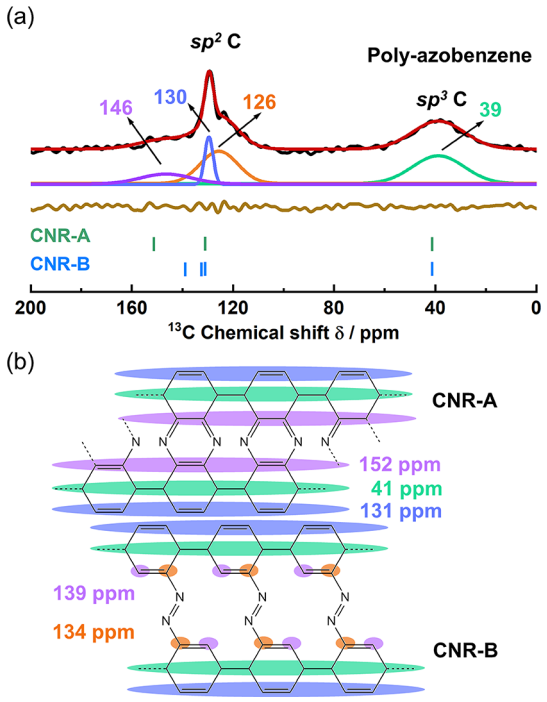

Figure 5. (a) ^{13}C CPMAS solid-state NMR spectrum of poly-azobenzene. The black, red, and brown lines represent the signal obtained from the experimental data, the deconvolution result, and the difference, respectively. The blue and green vertical lines represent the calculation NMR results of the CNR-A and CNR-B models, respectively. (b) Structure models of CNR-A and CNR-B. The assignments of the isotropic peaks are marked with corresponding colors to guide the eye.

black product presented obvious D and G bands at 1347 and 1582 cm^{-1}, respectively, which is a typical feature of a sp^2–sp^3 graphitic material. Similar results were also observed in in situ high-pressure IR spectra (Figures 2c and S5). Above 22 GPa, a new peak appeared at 2989 cm^{-1}. Meanwhile, the peaks centered at 827, 1528, and 1646 cm^{-1} broadened abruptly (marked in arrows in Figure 2c). These features marked the onset of the reaction, consistent with the literature.[30] When decompressed to ambient pressure, four new peaks were observed at 756, 1495, 1600, and 2997 cm^{-1} (marked in arrows in Figure 2c), which indicates the formation of new

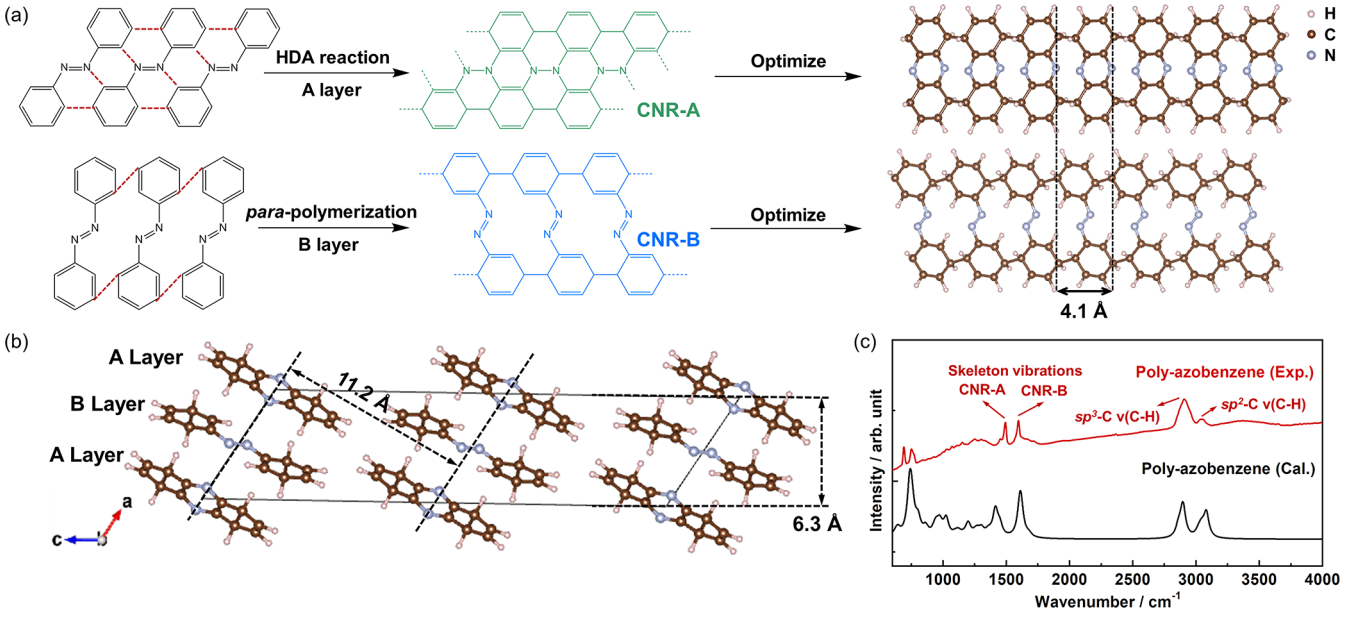

Figure 4. (a) Proposed HDA reactions in azobenzene of layer A and *para*-polymerization reactions in azobenzene of layer B as well as optimized CNR-A and CNR-B structures. (b) Crystal structure of poly-azobenzene. (c) IR spectra of poly-azobenzene from the experiment and calculation.

https://doi.org/10.1021/jacs.2c13753
J. Am. Chem. Soc. 2023, 145, 6845−6852

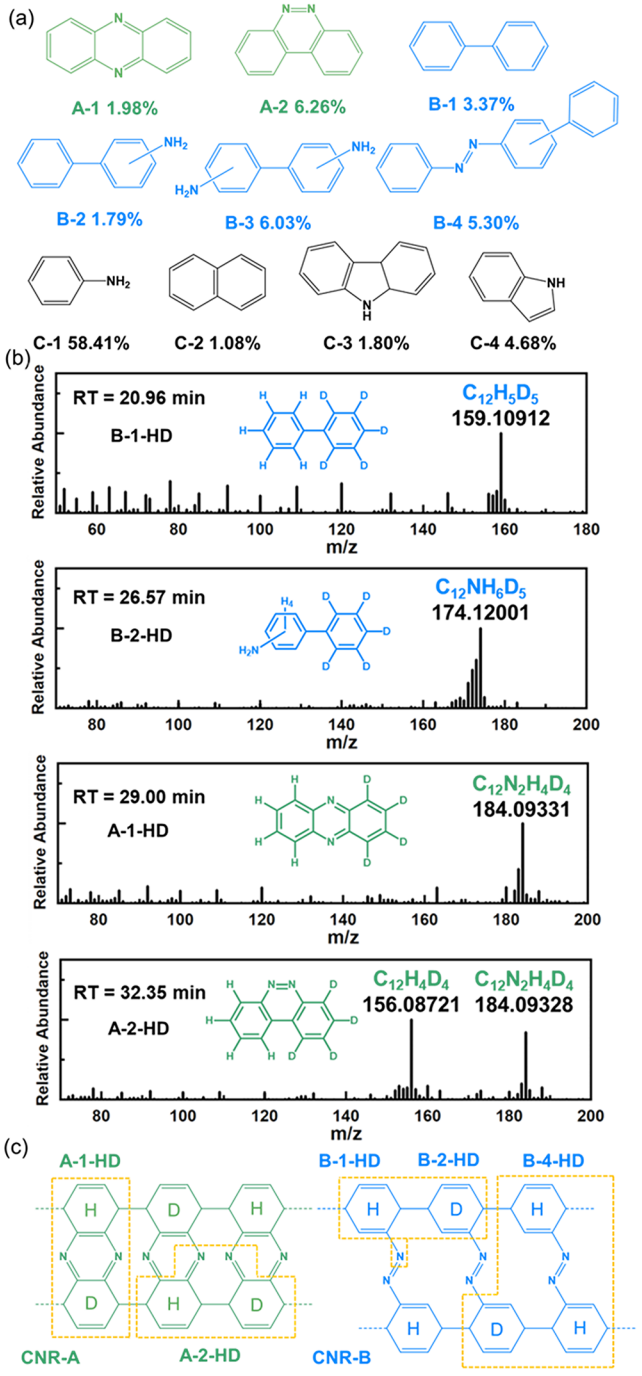

Figure 6. (a) Main oligomers detected in the poly-azobenzene recovered from 25 GPa by HRGC-MS and their content. (b) Mass spectra of the isotope-labeled oligomers and the corresponding molecular structures. Fused ring compounds drawn in green can be traced from the [4 + 2] hetero-Diels–Alder reaction product CNR-A, and biphenyl fragments drawn in blue can be traced from CNR-B. RT stands for the retention time. (c) Co-labeled oligomers by H and D detected in the PIP product of a 1:1 mixture of $C_{12}H_{10}N_2$–$C_{12}D_{10}N_2$ by HRGC-MS and the relationship between these compounds and CNR-A/CNR-B.

skeletons of carbon nanoribbon (CNR) and sp^3-C–H according to our latter calculations, and unambiguously demonstrates the reaction of phenyls.

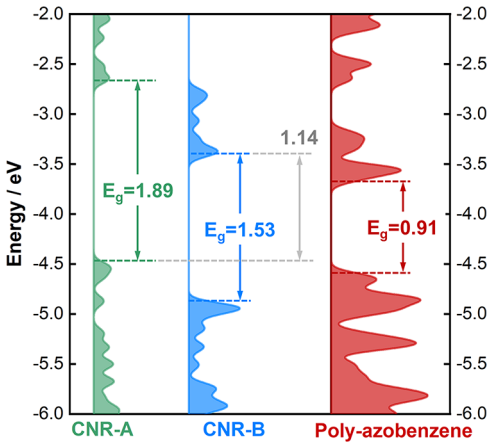

Figure 7. Calculated densities of states (DOS) of single-layered CNR-A and CNR-B as well as bulk poly-azobenzene. All energies are given with respect to the vacuum level.

The *trans*-azobenzene crystallizes in the monoclinic phase at ambient pressure ($P2_1/c$, a = 15.40 Å, b = 5.76 Å, c = 12.14 Å, and β = 114.08°). Its high-pressure structure evolution was then investigated by in situ synchrotron XRD up to 25 GPa (Figure 2d). By performing the Rietveld refinement, the lattice parameters were obtained (Figures S6 and S7), and the P–V relationship of azobenzene was then fitted by two third-order Birch–Murnaghan equation of state (EOS) (Figure 2e),[32] with V_0 = 917(8) Å^3, B_0 = 32(5) GPa, and B_1 = 3.8(8) below 11.5 GPa and V_0 = 865(55) Å^3, B_0 = 62(35) GPa, and B_1 = 2.0 (1.5) at higher pressure. This proves a possible phase transition of azobenzene around 10 GPa, consistent with the previous in situ XRD and spectroscopy measurements.[29−31] At 19.5 GPa, the intensity of the main peak of azobenzene at 7.7° decreased obviously, while the intensity of the diffraction peak at 7.3° increased. Meanwhile, there is a discontinuity of lattice parameters with pressure, which is likely due to the reaction. When compressed to 25 GPa, a new peak at 3.5° (10.9 Å) was detected, which remained during subsequential decompression to ambient pressure and was recognized as the characteristic peak of the polymerized azobenzene. Azobenzene also re-appeared when decompressed to ambient condition (Figure S8).

The crystal structure of azobenzene at the threshold pressure (17.1 GPa) was then optimized by density functional theory (DFT) calculation with the lattice parameters fixed at the result of Rietveld refinement (a = 13.35 Å, b = 5.21 Å, c = 11.03 Å, and β = 116.23°), and the obtained crystallographic data are presented in Table S2. As shown in Figure 2f, the molecules in layer A have the nearest intermolecular distances between phenyl and phenyl ($d_{C1\cdots C2'}$ = 3.03 Å), and phenyl and azo ($d_{C3\cdots N1'}$ = 3.37 Å), close to the threshold distance of the Diels–Alder reaction happened in 1,4-diphenylbutadiyne.[22] Such arrangement of molecules is suitable for a HDA reaction, in which the azophenyl acts as a "diene" and the phenyl acts as a "dienophile". In contrast, in layer B, molecules have the nearest intermolecular distances between phenyls (3.18 Å). The distances between azophenyl and phenyl are 4.79 Å ($d_{C4\cdots N2'}$) and 3.61 Å ($d_{C5\cdots C6'}$), respectively, which are too far for a HDA reaction.[22] As a result, the molecules in layer B should have "inert" azo groups due to inappropriate stacking and may bond via other routes, like the *para*-polymerization

https://doi.org/10.1021/jacs.2c13753
J. Am. Chem. Soc. 2023, 145, 6845–6852

between the adjacent phenyls.[33,34] This is consistent with the in situ Raman results mentioned before.

To understand the structure of polymerized products, we synthesized poly-azobenzene by Paris−Edinburgh (PE) Press at 20 GPa. Poly-azobenzene displays three sharp diffraction peaks at 11.2, 6.3, and 5.6 Å (Figure 3a). The selected area electron diffraction (SAED) pattern of poly-azobenzene indicated that these peaks are from the same phase, and indexed using a 2D-lattice with a = 7.67 Å, c = 27.13 Å, and β = 123.5° (Figure 3b). The ordering of b-axis was not found after many attempts, which is also a typical feature for the assembly of most nanothreads and nanoribbons.[17,20−22,35]

The sample morphology observed using scanning electron microscopy (SEM) and transmission electron microscopy (TEM) also suggests a 1-D ribbon structure (Figure 3d,e).[22] In addition, we found that the unit cells of the polymer and the monomer have almost the same area of the a−c plane (173.5 Å^2 for the polymer and 170.8 Å^2 for the monomer), which indicates that the ribbons are not bonded in the a−c plane. Therefore, we can conclude that azobenzene reacts along the b direction with the shortest intermolecular distance to form one-dimensional carbon−nitrogen nanoribbons.

Considering the appropriate intermolecular orientation and distance along the b axis of azobenzene crystal under critical pressure and the structural feature of poly-azobenzene, we proposed the azobenzene of layer A polymerizes into carbon−nitrogen nanoribbon-A (CNR-A) via HDA reactions and subsequential partly elimination of hydrogen, and the azobenzene of layer B polymerizes into carbon−nitrogen nanoribbon-B (CNR-B) via *para*-bonding of phenyl (Figure 4a). The crystal structure of poly-azobenzene was optimized with the lattice parameters a, c, and β fixed at the experimental results, and b = 4.1 Å was obtained in the optimization. No imaginary phonon mode was obtained in the calculation, which demonstrates the dynamical stability of this structure (Figure S9). The structures of CNR-A and CNR-B are shown in Figure 4a. In the optimized CNR-A, the N−N bonds (from the azo group) break and form phenazine units, reaching a locally stable state. The complete crystal structure of poly-azobenzene is shown in Figure 4b, with the lattice parameters and atomic coordinates listed in Table S3. The XRD pattern and SAED pattern simulated by the crystal structure fit the experimental data well (Figure 3a−c), which confirms the proposed model. The unit cell volume of poly-azobenzene is compressed by 28% compared to that of azobenzene due to the polymerization.

The proposed structure of the poly-azobenzene composite is also evidenced by IR and cross-polarization magic-angle-spinning (CPMAS) solid-state nuclear magnetic resonance (NMR). We calculated the IR spectrum of poly-azobenzene by DFT, which also fit the experimental data well. The two strong IR peaks at 1495 and 1600 cm^{-1} are ascribed to the skeleton vibrations of CNR-A (1413 cm^{-1}) and CNR-B (1612 cm^{-1}), respectively (Figures 4c and S10). The C(sp^3)−H and C(sp^2)−H stretching modes were identified at about 2900 and 3000 cm^{-1}, respectively, indicating that two types of C−H exist on the poly-azobenzene. The detailed assignments of the IR peaks are provided in Figure S10 according to the theoretical calculation.

The CPMAS solid-state NMR data of poly-azobenzene also shows the signals of sp^2 C and sp^3 C, which can be fitted by four peaks at 146, 130, 126, and 39 ppm, indicating three kinds of sp^2 C and one kind of sp^3 C presented in poly-azobenzene. The experimental results are also well reproduced by the theoretical simulation (vertical lines in Figure 5a) based on the proposed product model (Figure 5b). The broad peak at 146 ppm is ascribed to the sp^2−C(−N) atoms in CNR-A (152 ppm) and sp^2−C(−H) atoms at the center of CNR-B (139 ppm), while the peak at 130 ppm is attributed to the sp^2−C(−H) atoms on the edge of CNR-A and CNR-B (131 ppm). The sp^3 carbons in CNR-A and CNR-B were calculated to be resonant at 41 ppm and are observed experimentally around 39 ppm. The peak at 126 ppm may originate from the sp^2−C(−N) atoms in CNR-B (134 ppm).

To confirm the polymerization pathways from azobenzene to CNR-A and CNR-B, we extracted oligomers from the poly-azobenzene sample recovered from 25 GPa for high-resolution gas chromatography−mass spectrometry (HRGC-MS) measurement (Figures S11−S14). As shown in Table S4, 13 compounds with content greater than 1% were detected. Aniline (58.41%) is the decomposition product, which is also common in the HRGC-MS experiments of other C−N polymer systems.[21] Several typical compounds that were recognized in the National Institute of Standards and Technology (NIST) database are shown in Figure 6a. The fused ring (8.24%) and biphenyls (16.49%) molecules were recognized to produce from the proposed HDA and *para*-polymerization reaction, respectively.

For an in-depth investigation on the intermolecular reaction, we carried out a parallel experiment on the 1:1 mixture of $C_{12}H_{10}N_2$−$C_{12}D_{10}N_2$, and the identified molecules are similar to the unlabeled sample but with H−D co-labeled, like A-1-HD (phenazine-d_4), A-2-HD(benzo[h]cinnoline-d_4), B-1-HD (biphenyl-d_5), B-2-HD (2-aminobiphenyl-d_5 or 3-aminobiphenyl-d_5), and B-4-HD [phenyl-(2-phenylphenyl)diazene-d_5 or phenyl-(3-phenylphenyl)diazene-d_5], with MS in Figures 6b and S15. As shown in Figure 6c, fused ring fragments A-1-HD and A-2-HD are unambiguously from the HDA product CNR-A, while biphenyl fragments such as B-1-HD, B-2-HD, and B-4-HD result from the *para*-polymerization reaction product CNR-B. Our GC−MS findings are in perfect accordance with the proposed structural models and clarify the controversy about the reactivity of the azo group in azobenzene.[29−31]

Our experimental data are perfectly interpreted by the heterostructure model instead of the double-core nanothreads model[30,31] according to our intensive analysis. Further theoretical calculation shows that the band gap for CNR-A is 1.89 eV (from −4.53 to −2.64 eV) and that for CNR-B is 1.53 eV (from −4.92 to −3.39 eV) (Figure 7). The valence band maximum (VBM) of the CNR-B is lower than that of CNR-A by 0.39 eV, while the conduction band minimum (CBM) of CNR-B is lower than that of CNR-A by 0.75 eV. Such an heterostructure of CNR-A and CNR-B has a characteristic of the so-called type II or staggered band gap alignment, in which both the VBM and CBM of one semiconductor are higher than the other, and brings considerable interest for the application of photovoltaics or photocatalysis.[36,37] The energy gap between the VBM of CNR-A and the CBM of CNR-B is 1.14 eV, which is close to the band gap of the bulk poly-azobenzene heterostructure (0.91 eV, Figures 7 and S16). This indicates that the electron transition of poly-azobenzene is likely an inter-ribbon transition between CNR-A and CNR-B.

https://doi.org/10.1021/jacs.2c13753
J. Am. Chem. Soc. 2023, 145, 6845−6852

CONCLUSIONS

In summary, we conclude that the azobenzene experiences two distinct topochemical polymerization reactions at 18 GPa including the HDA reaction between the azophenyl and phenyl groups and the *para*-polymerization reaction between two phenyl moieties and produced an orderly stacked CNR van der Waals heterostructure. The different reaction selectivity is caused by the arrangement of the ABAB layer stacking in the crystal. This is the first example to produce the vdW heterostructure by using the PIP reaction from monomers with different stackings, which provides a novel and fresh perspective on the creation of bulk heterostructure materials.

ASSOCIATED CONTENT

Supporting Information

The Supporting Information is available free of charge at https://pubs.acs.org/doi/10.1021/jacs.2c13753.

Experimental procedures; characterization methods of in situ high-pressure Raman, IR, and XRD experiments; synthetic methods of poly-azobenzene; characterization of the sample poly-azobenzene by XRD, SEM, TEM, IR, CPMAS solid-state NMR, and GC−MS; optimization of crystal structure of azobenzene and construction of the structural models of poly-azobenzene; and calculation of phonon frequency, IR, NMR, band structures, and DOS (PDF)

AUTHOR INFORMATION

Corresponding Author

Kuo Li − *Center for High Pressure Science and Technology Advanced Research, Beijing 100193, People's Republic of China;* orcid.org/0000-0002-4859-6099; Email: likuo@hpstar.ac.cn

Authors

Peijie Zhang − *Center for High Pressure Science and Technology Advanced Research, Beijing 100193, People's Republic of China;* Present Address: Southern University of Science and Technology, Shenzhen, Guangdong 518055, People's Republic of China; orcid.org/0000-0001-6355-5482

Dexiang Gao − *Center for High Pressure Science and Technology Advanced Research, Beijing 100193, People's Republic of China;* Present Address: Institute of High Energy Physics, Chinese Academy of Sciences, 100049 Beijing, People's Republic of China.; Present Address: Spallation Neutron Source Science Center, Dongguan, Guangdong 523803, People's Republic of China.

Xingyu Tang − *Center for High Pressure Science and Technology Advanced Research, Beijing 100193, People's Republic of China*

Xin Yang − *Center for High Pressure Science and Technology Advanced Research, Beijing 100193, People's Republic of China*

Haiyan Zheng − *Center for High Pressure Science and Technology Advanced Research, Beijing 100193, People's Republic of China;* orcid.org/0000-0002-4727-5912

Yida Wang − *Center for High Pressure Science and Technology Advanced Research, Beijing 100193, People's Republic of China*

Xuan Wang − *Center for High Pressure Science and Technology Advanced Research, Beijing 100193, People's Republic of China;* Present Address: Institute of High Energy Physics, Chinese Academy of Sciences, 100049, Beijing, People's Republic of China.; orcid.org/0000-0001-6647-9542

Jingqin Xu − *Center for High Pressure Science and Technology Advanced Research, Beijing 100193, People's Republic of China*

Zijia Wang − *Center for High Pressure Science and Technology Advanced Research, Beijing 100193, People's Republic of China*

Jie Liu − *Center for High Pressure Science and Technology Advanced Research, Beijing 100193, People's Republic of China*

Xiaoge Wang − *College of Chemistry and Molecular Engineering, Peking University, Beijing 100871, People's Republic of China*

Jing Ju − *College of Chemistry and Molecular Engineering, Peking University, Beijing 100871, People's Republic of China*

Mingxue Tang − *Center for High Pressure Science and Technology Advanced Research, Beijing 100193, People's Republic of China;* orcid.org/0000-0002-7282-4100

Xiao Dong − *Key Laboratory of Weak-Light Nonlinear Photonics, School of Physics, Nankai University, Tianjin 300071, People's Republic of China;* orcid.org/0000-0003-4533-1914

Ho-kwang Mao − *Center for High Pressure Science and Technology Advanced Research, Beijing 100193, People's Republic of China*

Complete contact information is available at: https://pubs.acs.org/10.1021/jacs.2c13753

Author Contributions

○P.Z. and D.G. contributed equally to this paper. All authors have given approval to the final version of the manuscript.

Funding

This work was supported by the National Natural Science Foundation of China (grant nos. 22022101 and 21875006). The authors also acknowledge the support of the National Key Research and Development Program of China (2019YFA0708502). X. D. is thankful for the support of the Nature Science Foundation of Tianjin (Grant No. 20JCYBJC01530).

Notes

The authors declare no competing financial interest.

ACKNOWLEDGMENTS

The authors acknowledge the support of the National Natural Science Foundation of China (grant nos. 22022101 and 21875006). The authors also acknowledge the support of the National Key Research and Development Program of China (2019YFA0708502). This work was carried out with the support of 4W2 beamline at Beijing Synchrotron Radiation Facility and 15U1 beamline at Shanghai Synchrotron Radiation Facility. This study was partially supported by Synergic Extreme Condition User Facility (SECUF). X. D. is thankful for the support of the Nature Science Foundation of Tianjin (Grant No. 20JCYBJC01530).

REFERENCES

(1) Zhang, Z.; Lin, P.; Liao, Q.; Kang, Z.; Si, H.; Zhang, Y. Graphene-based mixed-dimensional van der Waals heterostructures for advanced optoelectronics. *Adv. Mater.* **2019**, *31*, 1806411.

(2) Wang, P.; Jia, C.; Huang, Y.; Duan, X. Van der Waals heterostructures by design: from 1D and 2D to 3D. *Matter* **2021**, *4*, 552−581.

(3) Bediako, D. K.; Rezaee, M.; Yoo, H.; Larson, D. T.; Zhao, S. Y. F.; Taniguchi, T.; Watanabe, K.; Brower-Thomas, T. L.; Kaxiras, E.; Kim, P. Heterointerface effects in the electrointercalation of van der Waals heterostructures. *Nature* **2018**, *558*, 425−429.

(4) Jiang, S.; Cheng, R.; Wang, X.; Xue, T.; Liu, Y.; Nel, A.; Huang, Y.; Duan, X. Realtime electrical detection of nitric oxide in biological systems with sub-nanomolar sensitivity. *Nat. Commun.* **2013**, *4*, 2225.

(5) Yu, W. J.; Liao, L.; Chae, S. H.; Lee, Y. H.; Duan, X. Toward tunable band gap and tunable Dirac point in bilayer graphene with molecular doping. *Nano Lett.* **2011**, *11*, 4759−4763.

(6) Zheng, J.-Y.; Xu, H.; Wang, J. J.; Winters, S.; Motta, C.; Karademir, E.; Zhu, W.; Varrla, E.; Duesberg, G. S.; Sanvito, S.; Hu, W.; Donegan, J. F. Vertical single-crystalline organic nanowires on graphene: solution-phase epitaxy and optical microcavities. *Nano Lett.* **2016**, *16*, 4754−4762.

(7) Dean, C. R.; Young, A. F.; Meric, I.; Lee, C.; Wang, L.; Sorgenfrei, S.; Watanabe, K.; Taniguchi, T.; Kim, P.; Shepard, K. L.; Hone, J. Boron nitride substrates for high-quality graphene electronics. *Nat. Nanotechnol.* **2010**, *5*, 722−726.

(8) Liu, Y.; Wang, F.; Wang, X.; Wang, X.; Flahaut, E.; Liu, X.; Li, L.; Wang, X.; Xu, Y.; Shi, Y.; Zhang, R. Planar carbon nanotube-graphene hybrid films for high-performance broadband photodetectors. *Nat. Commun.* **2015**, *6*, 8589.

(9) Zhang, J.; Lin, L.; Sun, L.; Huang, Y.; Koh, A. L.; Dang, W.; Yin, J.; Wang, M.; Tan, C.; Li, T.; Tan, Z.; Liu, Z.; Peng, H. Clean transfer of large graphene single crystals for high-intactness suspended membranes and liquid cells. *Adv. Mater.* **2017**, *29*, 1700639.

(10) Yan, M.; Wang, F.; Han, C.; Ma, X.; Xu, X.; An, Q.; Xu, L.; Niu, C.; Zhao, Y.; Tian, X.; Hu, P.; Wu, H.; Mai, L. Nanowire templated semihollow bicontinuous graphene scrolls: designed construction, mechanism, and enhanced energy storage performance. *J. Am. Chem. Soc.* **2013**, *135*, 18176−18182.

(11) Yoo, C.-S. Chemistry under extreme conditions: pressure evolution of chemical bonding and structure in dense solids. *Matter Radiat. Extremes* **2020**, *5*, 018202.

(12) Yang, X.; Wang, X.; Wang, Y.; Li, K.; Zheng, H. From molecules to carbon materials-high pressure induced polymerization and bonding mechanisms of unsaturated compounds. *Crystals* **2019**, *9*, 490.

(13) Wang, X.; Li, K.; Zheng, H.; Zhang, P. Chemical reactions of molecules under high pressure. *Chem. Bull.* **2019**, *82*, 387−398.

(14) Sun, J.; Dong, X.; Wang, Y.; Li, K.; Zheng, H.; Wang, L.; Cody, G. D.; Tulk, C. A.; Molaison, J. J.; Lin, X.; Meng, Y.; Jin, C.; Mao, H.-k. Pressure-induced polymerization of acetylene: structure-directed stereoselectivity and a possible route to graphane. *Angew. Chem., Int. Ed.* **2017**, *56*, 6553−6557.

(15) Wang, Y.; Dong, X.; Tang, X.; Zheng, H.; Li, K.; Lin, X.; Fang, L.; Sun, G.; Chen, X.; Xie, L.; Bull, C. L.; Funnell, N. P.; Hattori, T.; Sano-Furukawa, A.; Chen, J.; Hensley, D. K.; Cody, G. D.; Ren, Y.; Lee, H. H.; Mao, H.-k. Pressure-induced Diels-Alder reactions in C_6H_6-C_6F_6 cocrystal towards graphane structure. *Angew. Chem., Int. Ed.* **2019**, *58*, 1468−1473.

(16) Fitzgibbons, T. C.; Guthrie, M.; Xu, E. S.; Crespi, V. H.; Davidowski, S. K.; Cody, G. D.; Alem, N.; Badding, J. V. Benzene-derived carbon nanothreads. *Nat. Mater.* **2015**, *14*, 43−47.

(17) Li, X.; Baldini, M.; Wang, T.; Chen, B.; Xu, E. S.; Vermilyea, B.; Crespi, V. H.; Hoffmann, R.; Molaison, J. J.; Tulk, C. A.; Guthrie, M.; Sinogeikin, S.; Badding, J. V. Mechanochemical synthesis of carbon nanothread single crystals. *J. Am. Chem. Soc.* **2017**, *139*, 16343−16349.

(18) Wang, X.; Yang, X.; Wang, Y.; Tang, X.; Zheng, H.; Zhang, P.; Gao, D.; Che, G.; Wang, Z.; Guan, A.; Xiang, J.-F.; Tang, M.; Dong, X.; Li, K.; Mao, H.-k. From biomass to functional crystalline diamond nanothread: pressure-induced polymerization of 2,5-furandicarboxylic acid. *J. Am. Chem. Soc.* **2022**, *144*, 21837−21842.

(19) Nobrega, M. M.; Teixeira-Neto, E.; Cairns, A. B.; Temperini, M. L. A.; Bini, R. One-dimensional diamondoid polyaniline-like nanothreads from compressed crystal aniline. *Chem. Sci.* **2018**, *9*, 254−260.

(20) Dunning, S. G.; Zhu, L.; Chen, B.; Chariton, S.; Prakapenka, V. B.; Somayazulu, M.; Strobel, T. A. Solid-state pathway control via reaction-directing heteroatoms: ordered pyridazine nanothreads through selective cycloaddition. *J. Am. Chem. Soc.* **2022**, *144*, 2073−2078.

(21) Gao, D.; Tang, X.; Xu, J.; Yang, X.; Zhang, P.; Che, G.; Wang, Y.; Chen, Y.; Gao, X.; Dong, X.; Zheng, H.; Li, K.; Mao, H.-k. Crystalline $C_3N_3H_3$ tube (3,0) nanothreads. *Proc. Natl. Acad. Sci. U.S.A.* **2022**, *119*, e2201165119.

(22) Zhang, P.; Tang, X.; Wang, Y.; Wang, X.; Gao, D.; Li, Y.; Zheng, H.; Wang, Y.; Wang, X.; Fu, R.; Tang, M.; Ikeda, K.; Miao, P.; Hattori, T.; Sano-Furukawa, A.; Tulk, C. A.; Molaison, J. J.; Dong, X.; Li, K.; Ju, J.; Mao, H.-k. Distance-selected topochemical dehydro-Diels-Alder reaction of 1,4-diphenylbutadiyne toward crystalline graphitic nanoribbons. *J. Am. Chem. Soc.* **2020**, *142*, 17662−17669.

(23) Németh, P.; McColl, K.; Smith, R. L.; Murri, M.; Garvie, L. A. J.; Alvaro, M.; Pécz, B.; Jones, A. P.; Corà, F.; Salzmann, C. G.; McMillan, P. F. Diamond-graphene composite nanostructures. *Nano Lett.* **2020**, *20*, 3611−3619.

(24) Németh, P.; McColl, K.; Garvie, L. A. J.; Salzmann, C. G.; Murri, M.; McMillan, P. F. Complex nanostructures in diamond. *Nat. Mater.* **2020**, *19*, 1126−1131.

(25) Luo, K.; Liu, B.; Hu, W.; Dong, X.; Wang, Y.; Huang, Q.; Gao, Y.; Sun, L.; Zhao, Z.; Wu, Y.; Zhang, Y.; Ma, M.; Zhou, X. F.; He, J.; Yu, D.; Liu, Z.; Xu, B.; Tian, Y. Coherent interfaces govern direct transformation from graphite to diamond. *Nature* **2022**, *607*, 486−491.

(26) Shen, B.; Ji, Z.; Lin, Q.; Gong, P.; Xuan, N.; Chen, S.; Liu, H.; Huang, Z.; Xiao, T.; Sun, Z. Graphenization of diamond. *Chem. Mater.* **2022**, *34*, 3941−3947.

(27) Li, F.; Xu, J.; Wang, Y.; Zheng, H.; Li, K. Pressure-induced polymerization: addition and condensation reactions. *Molecules* **2021**, *26*, 7581.

(28) Brown, C. J. A refinement of the crystal structure of azobenzene. *Acta Crystallogr.* **1966**, *21*, 146−152.

(29) Dong, Z.; Seemann, N. M.; Lu, N.; Song, Y. Effects of high pressure on azobenzene and hydrazobenzene probed by Raman spectroscopy. *J. Phys. Chem. B* **2011**, *115*, 14912−14918.

(30) Romi, S.; Fanetti, S.; Alabarse, F.; Mio, A. M.; Bini, R. Synthesis of double core chromophore-functionalized nanothreads by compressing azobenzene in a diamond anvil cell. *Chem. Sci.* **2021**, *12*, 7048−7057.

(31) Romi, S.; Fanetti, S.; Alabarse, F.; Bini, R. Structure-reactivity relationship in the high-pressure formation of double-core carbon nanothreads from azobenzene crystal. *J. Phys. Chem. C* **2021**, *125*, 17174−17182.

(32) Birch, F. Finite strain isotherm and velocities for single-crystal and polycrystalline NaCl at high pressures and 300 K. *J. Geophys. Res.* **1978**, *83*, 1257−1268.

(33) Ciabini, L.; Santoro, M.; Gorelli, F. A.; Bini, R.; Schettino, V.; Raugei, S. Triggering dynamics of the high-pressure benzene amorphization. *Nat. Mater.* **2007**, *6*, 39−43.

(34) Chen, B.; Hoffmann, R.; Ashcroft, N. W.; Badding, J.; Xu, E.; Crespi, V. Linearly polymerized benzene arrays as intermediates, tracing pathways to carbon nanothreads. *J. Am. Chem. Soc.* **2015**, *137*, 14373−14386.

(35) Huang, H. T.; Zhu, L.; Ward, M. D.; Wang, T.; Chen, B.; Chaloux, B. L.; Wang, Q.; Biswas, A.; Gray, J. L.; Kuei, B.; Cody, G. D.; Epshteyn, A.; Crespi, V. H.; Badding, J. V.; Strobel, T. A. Nanoarchitecture through strained molecules: cubane-derived scaffolds and the smallest carbon nanothreads. *J. Am. Chem. Soc.* **2020**, *142*, 17944−17955.

https://doi.org/10.1021/jacs.2c13753
J. Am. Chem. Soc. 2023, 145, 6845−6852

(36) Lee, H.; Kim, S.; Chung, W.-S.; Kim, K.; Kim, D. Hybrid solar cells based on tetrapod nanocrystals: The effects of compositions and type II heterojunction on hybrid solar cell performance. *Sol. Energy Mater. Sol. Cells* **2011**, *95*, 446−452.
(37) Paul, T.; Das, D.; Das, B. K.; Sarkar, S.; Maiti, S.; Chattopadhyay, K. K. $CsPbBrCl_2$/g-C_3N_4 type II heterojunction as efficient visible range photocatalyst. *J. Hazard. Mater.* **2019**, *380*, 120855.

https://doi.org/10.1021/jacs.2c13753
J. Am. Chem. Soc. 2023, 145, 6845−6852